Effects of Mutual Coupling of Radiating Antennas on an Adaptive Radar Detector

Silvio De Nicola, Antonio De Maio, Alfonso Farina, Michele Fiorini, Leopoldo Infante, and Marco Piezzo

Abstract—In this paper, we address the adaptive detection/classification of signals in a homogenous interference environment. We refer to a radar system equipped with a phased array antenna and account for both the presence of mutual coupling between radiating antennas and a possible coherent interferer impinging on the array mainbeam. To deal with this scenario, we adopt a two-stage detection/classification scheme, enjoying the Costant False Alarm Rate (CFAR) property, to discriminate between target detection and coherent interferer rejection. Finally, we evaluate the system performance via Monte Carlo simulations. The results show that our system has interesting rejection capabilities and satisfactory detection levels. As a consequence, it could be successfully applied in real scenarios where mutual coupling is present.

Keywords—Adaptive radar detection, mutual coupling effects between radiating elements, constant false alarm rate, interference rejection.

I. INTRODUCTION

A Considerable amount of work has been directed towards the design of adaptive arrays for radar target detection and many algorithms have been proposed in open literature [1], [2].

Usually, at the design stage, it is assumed that an ideal array is available; hence real world effects, such as the mutual coupling between array elements, are sometimes neglected. Indeed, reflected radiation from one antenna element couples to its neighbors, as do currents that propagate along the surface of the array. As a consequence, mutual coupling arises, namely the voltage of each array element is the sum of the voltage due to the incident radiation, plus all the contributions from the various coupling sources from each of its neighbors. It is thus of primary concern to assess the impact of the aforementioned impairment on actual systems to quantify the possible performance loss. Some studies in this context can be found [3]–[5]. It is fundamental to exploit a mathematical model of the coupling effect as close as possible to the real phenomenon. We achieve this goal resorting to a suitable thorough electromagnetic model, highlighting the significant discrepancies between the ideal case and the operating situation.

Corresponding author S. De Nicola is with AGCOM, Centro Direzionale Isola B5, 80143, Naples, Italy (e-mail: s.denicola@agcom.it). The opinions expressed here are those of the author and do not necessarily reflect the positions of AGCOM.

A. De Maio and M. Piezzo are with Universitá di Napoli "Federico II", Via Claudio 21, 80125, Naples, Italy (e-mails: {ademaio,marco.piezzo}@unina.it).

A. Farina, M. Fiorini, and L. Infante are with SELEX Sistemi Integrati, Via Tiburtina km 12.4, 00131, Rome, Italy (e-mails: {afarina,mfiorini,linfante}@selex-si.com).

Additionally, to deal with the presence of a coherent interferer impinging on the array mainbeam, a possible approach might rely on modifying the null hypothesis in the detection test, which usually states that the vector under test contains clutter plus noise only, so that the observable can contain a coherent interfering vector too [6]. Other possibilities might be based on a multiple hypotheses framework [7] or on the design of schemes obtained cascading two detectors (*two-stage system*). Precisely, a useful signal detection is declared only when data survive two detection thresholding processes [8]–[10]. Following this approach, in this work we consider a two-stage detector, robust to the mutual coupling effect, whose first stage is a CFAR detector, as the Adaptive Matched Filter (AMF) [11], followed by a classification block discriminating between matched or mismatched signals [12].

At the analysis stage, we prove the effectiveness of the considered detector on a simulated subarray structure affected by mutual coupling and in the presence of coherent interfering signals. The proposed scheme, even in a non-ideal scenario, can adaptively trade detection capabilities for rejection properties of coherent interferer.

The paper is organized as follows: in Section II we describe the system model, explaining both the adopted mutual coupling model and the signal discrimination rule. In Section III, we deal with the performance analysis. Some conclusions and possible future researches are provided in Section IV.

A. Notation

We adopt the notation of using lower case boldface for vector a with elements $a(i)$, and upper case boldface for matrix A with entries $A(m,n)$. The conjugate, the transpose, and the conjugate transpose are denoted by the symbols $(\cdot)^*$, $(\cdot)^T$, and $(\cdot)^\dagger$ respectively. I and 0 denote the identity matrix and the matrix with zero entries (their size is determined from the context). For a square matrix X, $\text{diag}X$, $\det X$, and $\text{tr}X$ represent a vector of diagonal element of X, the determinant of X, and the trace of X, respectively. The letter j indicates the imaginary unit (i.e. $j = \sqrt{-1}$). For a complex number x, $|x|$ is the modulus of x. The symbol $\odot$ represents the Hadamard element-wise product. The statistical expectation is denoted by $E[\cdot]$. Finally, the curled inequality symbol $\succeq$ is used to denote generalized inequality: $A \succeq 0$ means that A is an Hermitian positive semidefinite matrix.

II. SYSTEM MODEL

A. Mutual Coupling Model

It is well known that the ideal radiation pattern of a large (compared to wavelength) planar array antenna, composed by
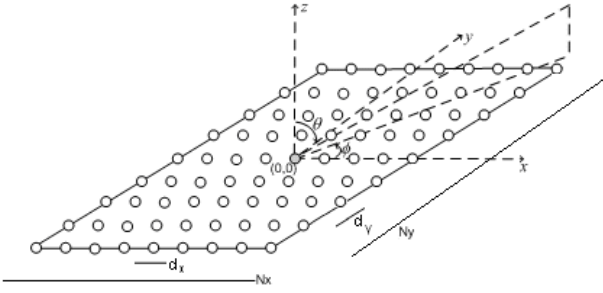
Fig. 1.   Array geometry and reference coordinates.

equal radiating elements, can be written as the product between the isolated (i.e. as in free space) single element pattern, supposed the same for all radiators, and the array factor, which is the only part that depends on the geometry of the array [13]. This ideal situation is not valid in real environments where many phenomena affect the theoretical electromagnetic propagation. Direct coupling by air radiation and substrate conducted waves, reflection by the array structure (including edge effects) are just a few among the impairments that a real antenna has to deal with. These aforementioned phenomena lead to the so called *mutual coupling effect* that is always present in a real array antenna. To evaluate such coupling effect on a real system, some methods have been developed in the past years, starting from the initial studies during the sixties by Galindo and Wu [14]. In the case of array composed by open ended waveguide radiators, the analytical method suggested by Borgiotti [15], [16] is one of the most prominent and it has been adopted and validated on real phased array antenna systems. The method is explained hereafter, while a more comprehensive and in-depth description of array design and field testing methods are found in Fenn's book on adaptive antennas and phased array antenna design [17].

As stated by Hannan [18], in a phased array antenna with a very large number of regularly-spaced radiating elements, the gain at the beam peak is equal to the number of elements times the gain obtained in the same direction by one isolated typical element of the array. Following Lechtreck [19], it is possible to consider as isolated typical element the central one located exactly in the centre of a large phased array antenna and then to derive for this element the isolated gain pattern $g_i^{(0,0)}$ (the symbols $(0,0)$ identify the central element, as shown in Figure 1. Since mutual coupling is inherently unavoidable when the elements are closely spaced (i.e. with spacing of the order of $\lambda/2$) [20], the active gain pattern for the central element is different from the ideal $g_i^{(0,0)}$. Pozar [21] showed the tight relationship between the active element pattern $g_a^{(0,0)}$ and the *active reflection coefficient* $\Gamma^{(0,0)}$ for the array scanned to the direction of interest defined by angles θ and ϕ,

$$g_a^{(0,0)} = g_i^{(0,0)} \left(1 - |\Gamma^{(0,0)}(\theta, \phi)|^2 \right). \tag{1}$$

Thus, for very large array compared to the wavelength λ, the gain of the active element embedded inside the array is seen as the directive aperture gain reduced by the mismatch loss due to the scanning. The active reflection coefficient of the central

antenna element $(0,0)$ can be computed using the following equation

$$\Gamma^{(0,0)}(\theta, \phi) = \sum_{n_x=-N_x}^{N_x} \sum_{n_y=-N_y}^{N_y} C_{n_x,n_y}^{(0,0)} e^{-j[n_x \psi_x(\theta,\phi) + n_y \psi_y(\theta,\phi)]}, \tag{2}$$

where $C_{n_x,n_y}^{(0,0)}$ are the mutual coupling coefficients between the central element $(0,0)$ and the (n_x, n_y) antenna with all other elements closed on matched terminations. The terms $\psi_x(\theta, \phi)$ and $\psi_y(\theta, \phi)$, provided by the array steering vector used, can be defined as $\psi_x(\theta, \phi) = 2\pi d_x \sin\theta \cos\phi/\lambda$ and $\psi_y(\theta, \phi) = 2\pi d_y \sin\theta \sin\phi/\lambda$, with d_x and d_y the distances of the (n_x, n_y) element from the central one $(0,0)$ (along axes x and y respectively). Note that an amplitude term related to the chosen array illumination could also be considered. This term is usually negligible, since common used illuminations are weakly tapered and thus the neighbouring elements can be assumed uniformly excited. As a result, it is useful in antenna design to know the active gain of the central element $(0,0)$ as a function of the scan angles and then, multiplying it by the array factor, the total radiated field by the array can be obtained. This permits to observe how the mutual coupling between the elements produce array blindness and pattern distortions in some specific angular regions. In our work, we are interested in the active gain of the element according to its actual position on the array. To this end, we have to refine the previously described model, considering the position dependent behaviour of the active element gain pattern. Since each radiating element perceives in general a different external environment, it happens that the mutual coupling coefficients of edge elements are different from the ones related to the central element. In the following, the mutual coupling coefficients have been derived via numerical electromagnetic simulator [22] according to the particular element position. Consequently, the active element pattern in the position (α, β) is found once the mutual coupling coefficients $C_{n_x,n_y}^{(\alpha,\beta)}$ are evaluated, with (n_x, n_y) varying on the remaining array elements. Then, using (2) and (1), it is possible to derive the active reflection coefficient $\Gamma^{(\alpha,\beta)}(\theta, \phi)$ and the active gain $g_a^{(\alpha,\beta)}(\theta, \phi)$, respectively. To reduce the complexity in the retrieval of the mutual coupling coefficients via time consuming electromagnetic numerical simulation some assumptions can be made. Considering the array homogeneity, it is possible to hypothesize that the coupling coefficients are invariant with respect to mutual translation as reported by Lechtreck [19]. Changing the position of the active element from (p_1, q_1) to (p_2, q_2), it is possible to re-use the same mutual coupling coefficients provided that the following condition is met: $C_{m_1,n_1}^{(p_1,q_1)} = C_{m_2,n_2}^{(p_2,q_2)}$ if $p_1 - m_1 = p_2 - m_2$ and $q_1 - n_1 = q_2 - n_2$. The active gain is still dependent upon the scan direction but also upon the location in the array since the mutual coupling coefficients are then summed in different ways by using (2). The above property for the mutual coupling coefficients is very useful to reduce the complexity of the problem without loss of generality. It is a common practice in phased array design to simulate or measure a certain number of mutual coupling coefficients for the central element pattern and then, resorting to extrapolation techniques, as those reported

by Galindo and Wu [14], it is possible to extrapolate them to the actual array size.

B. Classification Algorithm for Target Detection versus Coherent Interferer Rejection

The problem at hand is to discriminate between the disturbance (clutter plus noise) only hypothesis and the alternatives that a coherent target echo or a coherent interferer is present in the received signal, in addition to the disturbance. As customary, in order to cancel clutter and noise-like interference we assume that a set of secondary data, free of signal components and coherent interferers, but sharing the same statistical properties of the disturbance in the cell under test, is available (*homogeneous environment*). A natural approach to deal with the aforementioned problem relies on a two-stage scheme with the AMF as first stage (i.e. *detection block*); if the AMF statistic (T_{AMF}) is greater than a proper threshold η, set to guarantee the preassigned probability of false alarm (P_{fa}), the raw data is fed to a second stage (i.e. *classification block*) aimed at discriminating between H_1 and H_2 (see Figure 2 for a pictorial description). This second stage solves the following
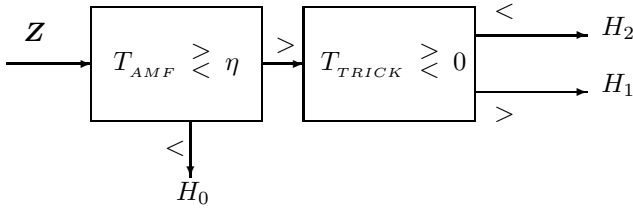

Fig. 2.   Block diagram of the AMF-TRICK.

hypothesis test

$$\begin{cases} H_1 : \begin{cases} \boldsymbol{z} = \alpha_1 \boldsymbol{p}(\zeta) + \boldsymbol{n}, & \zeta \in \mathcal{I}_1, \\ \boldsymbol{z}_k = \boldsymbol{n}_k, & k = 1, \dots, K, \end{cases} \\ H_2 : \begin{cases} \boldsymbol{z} = \alpha_2 \boldsymbol{p}(\zeta) + \boldsymbol{n}, & \zeta \in \mathcal{I}_2, \\ \boldsymbol{z}_k = \boldsymbol{n}_k, & k = 1, \dots, K, \end{cases} \end{cases}$$

where $\mathcal{I}_1 = [\zeta_0 - \zeta_\epsilon, \zeta_0 + \zeta_\epsilon]$, $\mathcal{I}_2 = \mathcal{I}_L \cup \mathcal{I}_U$, $\mathcal{I}_L = [\zeta_0 - \pi, \zeta_0 - \zeta_\epsilon]$, $\mathcal{I}_U = [\zeta_0 + \zeta_\epsilon, \zeta_0 + \pi]$, α_1 and α_2 unknown parameters accounting for the possible signal uncertain complex amplitude, $E[\boldsymbol{n}\boldsymbol{n}^\dagger] = E[\boldsymbol{n}_k\boldsymbol{n}_k^\dagger] = \boldsymbol{R}$ is the unknown disturbance covariance matrix, and $\boldsymbol{p}(\zeta) = 1/\sqrt{M}[1 \ e^{j\zeta} \cdots e^{j(M-1)\zeta}]^T$ is the ideal array steering vector structure. Finally, the parameter $\zeta_\epsilon \in (0, \pi)$ rules the size of the acceptance region, centered around the nominal ζ_0. To cope with the *a priori* uncertainty about the unknown parameters, we resort to the Generalized Maximum Likelihood (GML) criterion, which is tantamount to implementing the following decision rule

$$\frac{\max\limits_{\zeta \in \mathcal{I}_1} \max\limits_{\alpha_1, \boldsymbol{R}} f_1(\boldsymbol{Z}; \boldsymbol{\Xi}_1)}{\max\limits_{\zeta \in \mathcal{I}_2} \max\limits_{\alpha_2, \boldsymbol{R}} f_2(\boldsymbol{Z}; \boldsymbol{\Xi}_2)} \underset{H_2}{\overset{H_1}{\gtrless}} \frac{p_2}{p_1} = 1,$$

where $\boldsymbol{Z} = [\boldsymbol{z} \ \boldsymbol{z}_1 \cdots \boldsymbol{z}_K]$ is the overall data matrix, for $i \in \{1, 2\}$, $\boldsymbol{\Xi}_i = [\alpha_i, \boldsymbol{R}, \zeta]$ is the vector of the unknown parameters under the H_i hypothesis, $p_i = 1/2$ is the *a-priori* probability of H_i, while $f_i(\boldsymbol{Z}; \boldsymbol{\Xi}_i)$ denotes the probability density function of the observables under the H_i hypothesis. Previous assumptions imply that

$$f_i(\boldsymbol{Z}; \boldsymbol{\Xi}_i) = \left[\frac{1}{\pi^N \det \boldsymbol{R}} e^{-\text{tr}(\boldsymbol{R}^{-1}\boldsymbol{T}_i)} \right]^{K+1}$$

where $\boldsymbol{T}_i$ is defined as

$$\boldsymbol{T}_i = \frac{1}{K+1} \left\{ [\boldsymbol{z} - \alpha_i \boldsymbol{p}(\zeta)] [\boldsymbol{z} - \alpha_i \boldsymbol{p}(\zeta)]^\dagger + \sum_{k=1}^K \boldsymbol{z}_k \boldsymbol{z}_k^\dagger \right\}$$

Maximazing over $\boldsymbol{R}$, α_1, and α_2, the proposed decision rule can be recast, after some algebra, as

$$T_{TRICK} = \max_{\zeta \in \mathcal{I}_1} F(\zeta) - \max_{\zeta \in \mathcal{I}_2} F(\zeta) \underset{H_2}{\overset{H_1}{\gtrless}} 0, \qquad (3)$$

with $F(\zeta) = |\boldsymbol{z}^\dagger \boldsymbol{S} \boldsymbol{p}(\zeta)|^2 / (\boldsymbol{p}(\zeta)^\dagger \boldsymbol{S} \boldsymbol{p}(\zeta))$, where $\boldsymbol{S} = \left(\sum_{k=1}^K \boldsymbol{z}_k \boldsymbol{z}_k^\dagger \right)^{-1}$. The statistic (3) can be evaluated exploiting the *hidden convexity* of the problem [23]. More precisely, the second stage decision rule, referred to as TRICK (*Trigonometric Classifier*), has been derived [12] as $T_{TRICK} = v(\mathcal{P}_1) - v(\mathcal{P}_2)$, where $v(\mathcal{P}_i)$ is the optimal value of the convex optimization problem $\mathcal{P}_i$. Since $v(\mathcal{P}_2) = \max\{v(\mathcal{P}_L), v(\mathcal{P}_U)\}$, it is necessary to solve the following convex problems $\mathcal{P}_i$ (with $i \in \{1, L, U\}$)

$$\mathcal{P}_i \begin{cases} \underset{t, \boldsymbol{X}_A, \boldsymbol{X}_B}{\text{minimize}} & t \\ \text{subject to} & t\boldsymbol{y} - \boldsymbol{x} = \boldsymbol{W}_A^\dagger (\text{diag}\boldsymbol{W}_A + \boldsymbol{d}_i \odot \text{diag}\boldsymbol{W}_B) \\ & t \in \mathbb{R} \\ & \boldsymbol{X}_A \succeq \boldsymbol{0} \\ & \boldsymbol{X}_B \succeq \boldsymbol{0}, \end{cases}$$

$$(4)$$

with $\boldsymbol{W}_A = \boldsymbol{W}_\alpha \boldsymbol{X}_A \boldsymbol{W}_\alpha^\dagger$, $\boldsymbol{W}_B = \boldsymbol{W}_\beta \boldsymbol{X}_B \boldsymbol{W}_\beta^\dagger$, $\boldsymbol{W}_\alpha = [\boldsymbol{W}_\beta \ \boldsymbol{w}_{M-1}] = [\boldsymbol{w}_0 \cdots \boldsymbol{w}_{M-2} \ \boldsymbol{w}_{M-1}]$, while $\boldsymbol{y}$, $\boldsymbol{x}$, $\boldsymbol{w}_k$, and $\boldsymbol{d}_i$ can be expressed as

$$\boldsymbol{y}(k) = \frac{1}{M} \sum_{n=1}^{M-k} \boldsymbol{S}(n+k, n),$$

$$\boldsymbol{x}(k) = \frac{1}{M} \sum_{n=1}^{M-k} \boldsymbol{r}(n+k)\boldsymbol{r}^*(n),$$

$$\boldsymbol{w}_k = [1 \ e^{-jk\omega} \cdots e^{-j(\mathcal{L}-1)k\omega}]^T,$$

$$\boldsymbol{d}_i(l) = \cos(\omega l - \zeta_i) - \cos\gamma_i, \ l = 0, \dots, \mathcal{L}-1,$$

with $k = 0, \dots, M-1$, $\boldsymbol{r} = \boldsymbol{S}\boldsymbol{z}$, $\zeta_1 = \zeta_0$, $\zeta_0 - \zeta_L = \zeta_U - \zeta_0 = (\zeta_\epsilon + \pi)/2$, $\gamma_1 = \zeta_\epsilon$, $\gamma_L = \gamma_U = \pi - \zeta_\epsilon$, and $\omega = 2\pi/\mathcal{L}$ for $\mathcal{L} \geq 2M - 1$ [12].

III. NUMERICAL SIMULATIONS

To apply the classification algorithm presented in Section II-B, a subarray antenna architecture [2], derived from the general planar one of Figure 1, is considered. More precisely, in Figure 3, we have considered a 32 element square

$(N_x = N_y = 32)$ antenna aperture with half-wavelength spacing $(d_x = d_y = d = \lambda/2)$, and 11 GHz carrier frequency. The aperture is tailored in $M = 8$ equal subarrays, disposed
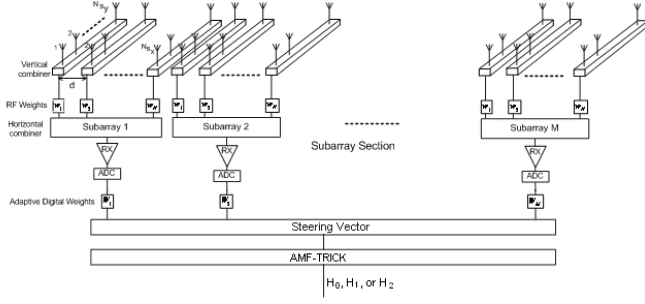

Fig. 3. Adaptive subarray antenna architecture.

along the horizontal plane. Each subarray is composed by $N_{S_x} \times N_{S_y}$ (4×32) radiating elements grouped column-wise using a passive vertical combiner which also narrows the beam along the elevation plane. The output of each vertical combiner is then forwarded to a set of weights that can be applied in the Radio Frequency (RF) stage by using, for instance, an active Transmit Receive Module (TRM). The subarrays are then formed combining 4 TRMs by using an horizontal combiner and then forwarding the received signal to the receiving chain, namely the receiver (RX) block followed by an Analog to Digital Converter (ADC). Finally, the classification algorithm of Section II-B is implemented based on the digital outputs of the available 8 channels.

The effects of the mutual coupling is modelled here as explained in the previous Section II-A for each single element of the array. Following the subarray architecture, the effective subarray antenna pattern is evaluated as the average of all the active element patterns belonging to that particular subarray. By doing so, the active electric field pattern of the m-th subarray $f_a^m(\theta, \phi)$ is the average of all the active electric fields by the elements belonging to that particular subarray, i.e.

$$f_a^m(\theta, \phi) = \frac{1}{N_{S_x} N_{S_y}} \sum_{(n_x, n_y) \in m\text{-th subarray}} f_a^{(n_x, n_y)}(\theta, \phi).$$

Following Pozar [21], the active electric field $f_a^{(n_x, n_y)}(\theta, \phi)$ by the (n_x, n_y) radiating element belonging to the m-th subarray is related to the active reflection coefficient whose expression is similar to (1)

$$f_a^{(n_x, n_y)}(\theta, \phi) = f_0(\theta, \phi)\left(1 + \Gamma^{(n_x, n_y)}(\theta, \phi)\right),$$

where the isolated electric field pattern is defined by $f_0(\theta, \phi)$. The average active element electric field patterns $f_a^m(\theta, \phi)$ are reported in Figure 4 for the edge $(m = 1)$ and in Figure 5 for the central $(m = 4)$ subarrays, adopting angular coordinates (θ_{EL}, ϕ_{AZ}) (related to spherical coordinates (θ, ϕ) by the formulas $\sin\theta\cos\phi = \cos\theta_{EL}\sin\phi_{AZ}$ and $\sin\theta\sin\phi = \sin\theta_{EL}$). In our phased array architecture, we have also considered two possible weights w_{n_x} and W_m, which depend on steering direction, say θ_0: in fact, to steer the array at angle θ_0, we can apply as illuminations $w_{n_x} = \alpha_{n_x}e^{-j2\pi(n_x-1)d\sin\theta_0/\lambda}$, for $n_x = 1, \ldots, N_{S_x}$ and
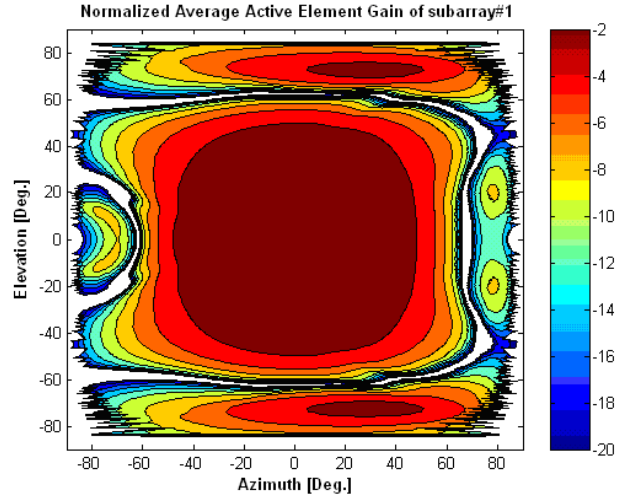

Fig. 4. Normalized contour plot of average active element pattern $f_a^m(\theta, \phi)$ for edge subarray $m = 1$ as a function of azimuth and elevation angles ϕ_{AZ} and θ_{EL}.
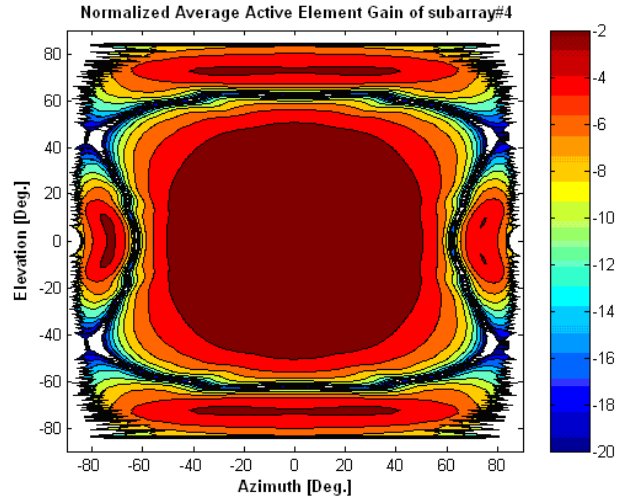

Fig. 5. Normalized contour plot of average active element pattern $f_a^m(\theta, \phi)$ for central subarray $m = 4$ as a function of azimuth and elevation angles ϕ_{AZ} and θ_{EL}.

$$W_m = A_m e^{-j2\pi(m-1)N_{S_x}d\sin\theta_0/\lambda}, \text{ for } m = 1, \ldots, M.$$
Finally, the M digital outputs are expressed by

$$W_m f_a^m(\theta, \phi)e^{j(m-1)N_{S_x}\psi_x(\theta,\phi)} \times$$

$$\left[\sum_{n_x=1}^{N_{S_x}}\sum_{n_y=1}^{N_{S_y}} w_{n_x} e^{j[(n_x-1)\psi_x(\theta,\phi)+(n_y-1)\psi_y(\theta,\phi)]}\right], \tag{5}$$

for $m = 1, \ldots, M$. These M subarray radiation patterns (along the azimuth cut) are reported in Figures 6-7 for two different scanning directions (respectively 0º and 20º). In these figures, the ideal case is kept as reference and the actual case, including mutual coupling, produces variations of the subarray antenna pattern in the sidelobe region and a beam pointing error of ± 1.5º. Considering the processing in the azimuth plane (i.e. $\phi = 0$º), we can rewrite (5) as
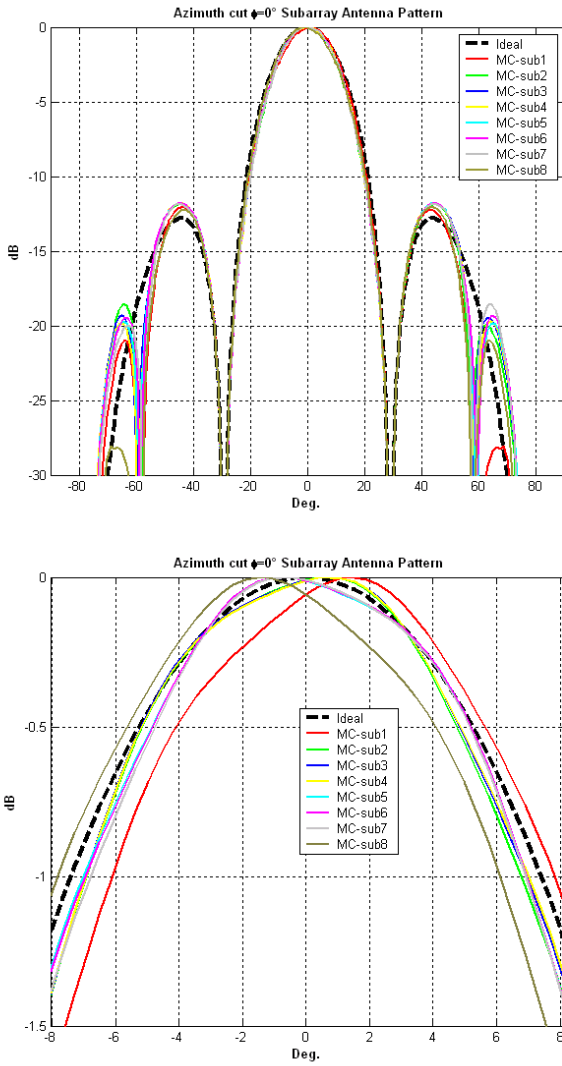
$$W_m f_{sub}^m(\theta, 0).$$

Fig. 6.   Top figure: normalized subarray antenna patterns with mutual coupling (solid lines) and as reference the ideal case (dashed-line) for 0º as scan direction. Lower figure: highlighted section zooming the peak gain to show the beam-pointing error of the subarray antenna pattern including mutual coupling effects.

Fig. 7.   Top figure: normalized subarray antenna patterns with mutual coupling (solid lines) and as reference the ideal case (dashed-line) for 20º as scan direction. Lower figure: highlighted section zooming the peak gain to show the beam-pointing error of the subarray antenna pattern including mutual coupling effects.

Finally, we have collected $f_{sub}^m(\theta, 0)$ into vectors $[f_{sub}^1(\theta, 0) \cdots f_{sub}^M(\theta, 0)]^T$ for two possible scanning directions (0º and 20º, as showed in the previous Figures 6-7). In both cases we have normalized these vectors, which have been referred to as $\boldsymbol{p}_{mc}(\zeta)$.

To evaluate the system performance, we analyze the probability of target detection, i.e.

$$P_d(\zeta) = P(H_1 | \text{a signal from the observation angle } \zeta)$$

for a given probability of false alarm $P_{fa} = P(H_1|H_0) + P(H_2|H_0)$. Since a closed formula is not available, we resort to standard Monte Carlo counting techniques to analyze the performance of the AMF-TRICK (the thresholds necessary to ensure the preassigned P_{fa} and the P_d are evaluated by resorting to $100/P_{fa}$ and $100/P_d$ independent trials, respectively). Finally, we use the toolbox SeDuMi [24], together with the Yalmip interface [25], to solve the SDPs (4). We
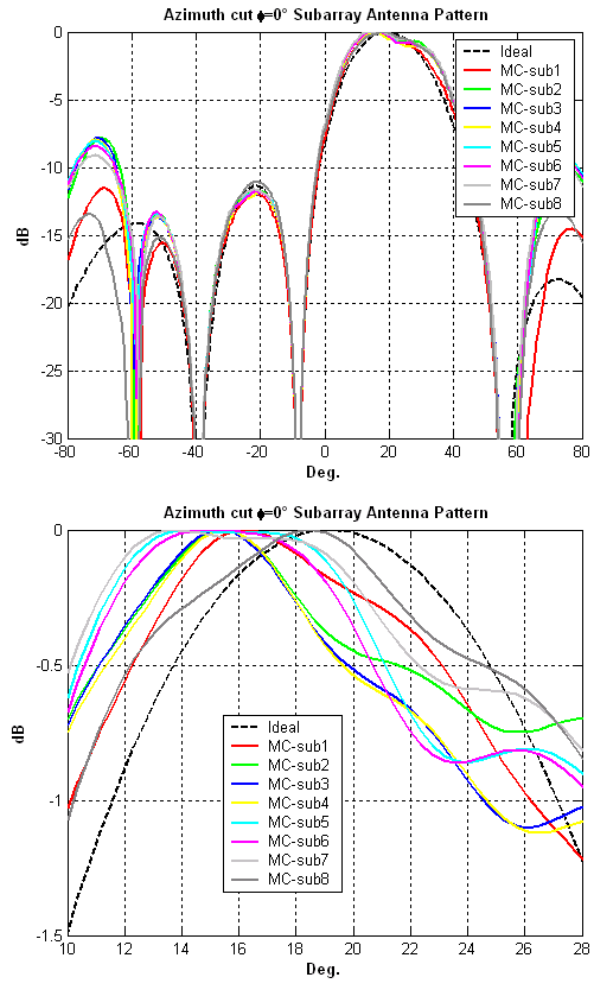
assume $K = 3M$, and $P_{fa} = 10^{-4}$. Moreover, we model the (complex normal) disturbance vectors according to the following covariance matrix $\boldsymbol{R} = \boldsymbol{I} + \sum_{u=1}^{I} \sigma_u^2 \boldsymbol{p}_{mc}(\zeta_u) \boldsymbol{p}_{mc}^\dagger(\zeta_u)$, where I is the number of noise-like interferers, σ_u^2 and ζ_u denote the interference-to-white-noise power ratio (IWNR) and the angle of arrival of the u-th interferer, respectively. In particular, we assume $I = 2$ interferers with the same IWNR equal to 10 dB, $[\zeta_1 \ \zeta_2] = [14.78º \ 29.58º]$, while the nominal signal-to-noise power ratio (SNR) is defined as $\text{SNR} = |\alpha|^2 \boldsymbol{p}_{mc}(\zeta_0)^\dagger \boldsymbol{R}^{-1} \boldsymbol{p}_{mc}(\zeta_0)$, with $\zeta_0 = 0º$. Finally, we compare the performance of the AMF-TRICK with the classic AMF [11] (i.e. just the first stage of the proposed detector), Kelly's GLRT [26], and W-ABORT [8], whose thresholds, evaluated through Monte Carlo counting techniques, have been set in order to guarantee the same P_{fa}.

Assuming 0º as scan direction, in Figure 8, we plot $P_d(\zeta_0)$ versus SNR for the proposed receivers. For the AMF-TRICK, we use several values of ζ_ϵ. Notice that decreasing ζ_ϵ, is tantamount to reducing the detection performance. Such a
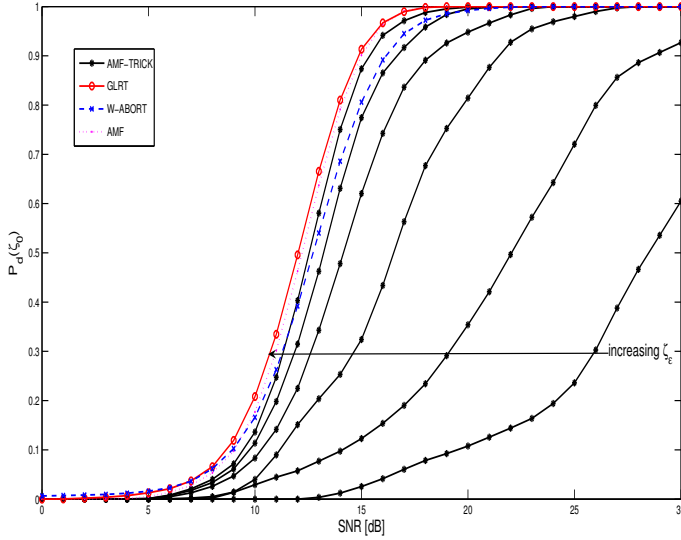
Fig. 8. $P_d(\zeta_0)$ versus SNR with 0º as scan direction for the AMF-TRICK (star solid curves), W-ABORT (x dot-dashed curves), GLRT (circle solid curve), and AMF (dot-dashed curves), $\zeta_\epsilon = [1.25º, 2.5º, 5º, 10º, 15º, 20º]$.

Fig. 9. $P_d(\zeta)$ versus ζ with SNR= 20 dB with 0º as scan direction for the AMF-TRICK (star solid curves), W-ABORT (x dot-dashed curves), GLRT (circle solid curve), and AMF (dot-dashed curves), $\zeta_\epsilon = [1.25º, 2.5º, 5º, 10º, 15º, 20º]$.

behavior was indeed expected: as the capabilities of the system to reject a coherent interferer improve, we experience a decrease in terms of matched target detection capabilities. However, for high values of ζ_ϵ, the GLRT, the W-ABORT and the AMF-TRICK are comparable. Moreover, for $\zeta_\epsilon \geq 20º$ the AMF and the AMF-TRICK almost coincide: this means that in this situation the classification stage does not affect the detection of a matched signal. In Figure 9, we study the discrimination capabilities of the proposed receiver. We plot $P_d(\zeta)$ versus ζ for SNR = 20 dB. For the AMF-TRICK, we consider different values of the design parameter ζ_ϵ. We can observe that increasing ζ_ϵ leads to higher values of $P_d(\zeta)$: since ζ_ϵ rules the angular discrimination of the classifier, higher values of T_{TRICK} can be achieved increasing ζ_ϵ (i.e. enlarging $\mathcal{I}_1$ and reducing $\mathcal{I}_2$). While AMF and GLRT have poor rejection performance, W-ABORT and AMF-TRICK can ensure interference rejection in the scanning region. Notably, reducing ζ_ϵ, AMF-TRICK can also reject a signal interference even in the mainbeam region.

This behaviour is confirmed when we assume a different scan direction (i.e. $\zeta_0 = 20º$). In Figure 10, we plot $P_d(\zeta_0)$ versus SNR for the proposed receiver. We can observe that the detection performance of AMF-TRICK is not affected by changing scan direction, coherently with other studies [6], [27]. Interestingly, as highlighted in Figure 11, AMF-TRICK ensures also in this case a good rejection of coherent interfering signals, although the effect of mutual coupling is more marked than $\zeta_0 = 0º$.

Summarizing, this analysis shows that in general the AMF-TRICK algorithm seems to ensure a better *detection-rejection* trade-off than other receivers, i.e. achieving a better selectivity (a narrower region of angular acceptance) for a given P_d. This gain is paid by an increased computational complexity of the system, since the AMF-TRICK requires solving convex SDP
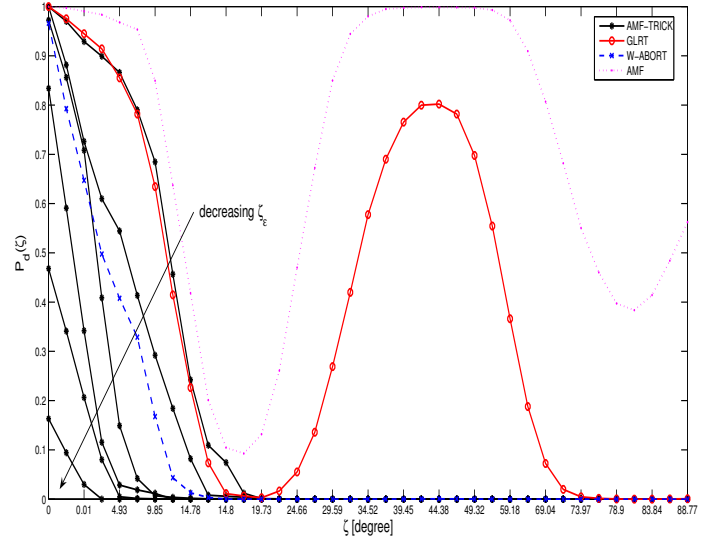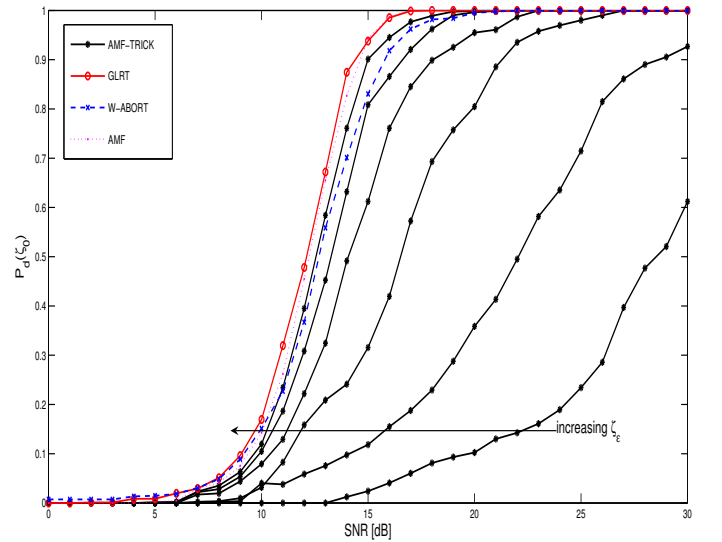

Fig. 10. $P_d(\zeta_0)$ versus SNR with 20º as scan direction for the AMF-TRICK (star solid curves), W-ABORT (x dot-dashed curves), GLRT (circle solid curve), and AMF (dot-dashed curves), $\zeta_\epsilon = [1.25º, 2.5º, 5º, 10º, 15º, 20º]$.

optimization problems [28].

IV. CONCLUSIONS

In this paper, we have proposed a strategy to detect the signal of interest in the presence of mutual coupling and coherent interferers. To this end, we have adopted a suitable electromagnetic model to describe the phased array steering vector and a two-stage detector to discriminate mainlobe and sidelobe signals. The analysis, conducted via numerical simulations, shows that our system could be successfully applied
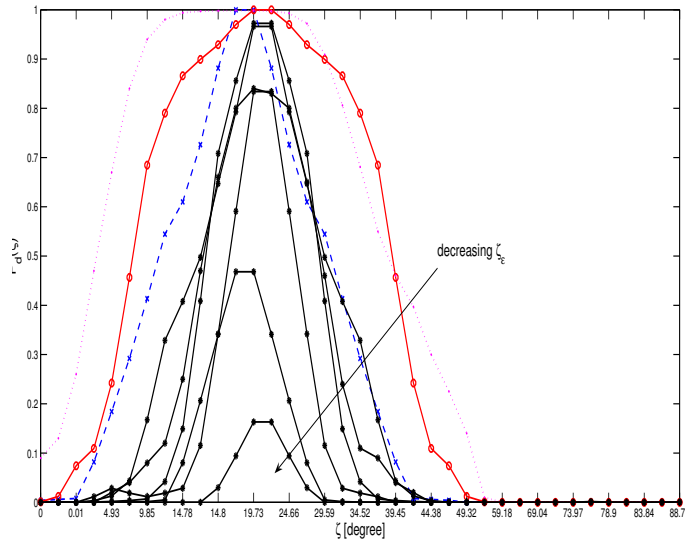
Fig. 11. $P_d(\zeta)$ versus ζ with SNR= 20 dB with 20º as scan direction for the AMF-TRICK (star solid curves), W-ABORT (x dot-dashed curves), GLRT (circle solid curve), and AMF (dot-dashed curves), $\zeta_\epsilon = [1.25º, 2.5º, 5º, 10º, 15º, 20º]$.

in real scenarios, where mutual coupling in the phased array antenna needs to be accounted for. Future possible researches might concern the extension of the trigonometric classifier to a bi-dimensional antenna subarray configuration, and/or to a real data analysis.

REFERENCES

[1] A. Farina, *Antenna-based signal processing techniques for radar systems*. Artech House, 1992.

[2] ——, "Electronic counter-countermeasures," in *M. Skolnik, Radar handbook*. McGraw Hill, 2008, ch. IX.

[3] A. De Maio, A. Farina, M. Fiorini, and A. Morini, "Performance analysis of sidelobe blanking system in presence of mutual coupling," in *Proceedings of IET Radar Conference*, Edinburgh (UK), October 2007, pp. 1–5.

[4] A. De Maio, L. Landi, and A. Farina, "Adaptive radar detection in the presence of mutual coupling and near-field effects," *IET Radar, Sonar & Navigation*, vol. 2, pp. 17–24, February 2008, issue n.1.

[5] G. Foglia, D. Marcantoni, F. Trotta, and A. De Maio, "ECM counteracting SLB: analysis and effectiveness evaluation," in *Proceedings of IEEE Radar Conference*, Rome (IT), 2008, pp. 1–6.

[6] S. De Nicola, A. De Maio, and A. Farina, "Robust adaptive detection with angular rejection," *Proceedings of SPIE*, vol. 7502, pp. 1–7, August 2009, issue n.1.

[7] F. Bandiera, A. Farina, D. Orlando, and G. Ricci, "Detection algorithms to discriminate between targets and ECM signals," *IEEE Transactions on Signal Processing*, vol. 58, pp. 5984–5993, December 2010, issue n.12.

[8] F. Bandiera, O. Besson, D. Orlando, and G. Ricci, "An improved adaptive sidelobe blanker," *IEEE Transactions on Signal Processing*, vol. 56, pp. 4152–4161, September 2008, issue n.9.

[9] C. D. Richmond, "Performance of the adaptive sidelobe blanker detection algorithm in homogeneous environments," *IEEE Transactions on Signal Processing*, vol. 48, pp. 1235–1247, May 2000, issue n.5.

[10] A. De Maio, "Rao test for adaptive detection in gaussian interference with unknown covariance matrix," *IEEE Transactions on Signal Processing*, vol. 55, pp. 3577–3584, July 2007, issue n.7.

[11] I. S. Reed, J. D. Mallett, and L. E. Brennan, "Rapid convergence rate in adaptive arrays," *IEEE Transactions on Aerospace and Electronic Systems*, vol. 10, pp. 853–863, November 1974, issue n.6.

[12] F. Bandiera, A. De Maio, S. De Nicola, A. Farina, D. Orlando, and G. Ricci, "Adaptive strategies for discrimination between mainlobe and sidelobe signals," in *Proceedings of IEEE Radar Conference*, Washington DC (USA), May 2010, pp. 910–914.

[13] C. A. Balanis, *Antenna theory analysis and design*. Wiley Interscience, 2005.

[14] V. Galindo and C. P. Wu, "On the asymptotic decay of coupling for infinite phased arrays," *Proceedings of the IEEE*, vol. 56, pp. 1872–1880, November 1968, issue n.11.

[15] G. V. Borgiotti, "Modal analysis of periodic planar phased arrays of apertures," *Proceedings of the IEEE*, vol. 56, pp. 1881–1892, November 1968, issue n.11.

[16] ——, "A novel expression for the mutual admittance of planar radiating elements," *IEEE Transactions on Antennas and Propagation*, vol. 16, pp. 329–333, May 1968, issue n.3.

[17] A. J. Fenn, *Adaptive antennas and phased arrays for radar and communications*. Artech House, 2007.

[18] P. W. Hannan, "The element-gain paradox for a phased array antenna," *IEEE Transactions on Antennas and Propagation*, vol. 12, pp. 423–433, July 1964, issue n.4.

[19] L. W. Lechtreck, "Effects of coupling accumulation in antenna arrays," *IEEE Transactions on Antennas and Propagation*, vol. 16, pp. 31–37, January 1968, issue n.1.

[20] N. Amitay, V. Galindo, and C. P. Wu, *Theory and analysis of phased array antennas*. Wiley Interscience, 1972.

[21] D. M. Pozar, "The active element pattern," *IEEE Transactions on Antennas and Propagatio*, vol. 42, pp. 1176–1178, August 1994, issue n.8.

[22] "CST Microwave Studio," http://www.cst.com.

[23] T. Roh and L. Vandenberghe, "Discrete transforms, semidefinite programming and sum-of-squares representations of nonnegative polynomials," *SIAM Journal on Optimization*, vol. 16, pp. 939–964, July 2006, issue n.4.

[24] J. F. Sturm, "Using SeDuMi 1.02, a MATLAB toolbox for optimization over symmetric cones," *Optimization Methods and Software*, vol. 11, no. 12, pp. 625–653, 1999.

[25] J. Löfberg, "YALMIP: A toolbox for modeling and optimization in MATLAB," in *IEEE International Symposium on Computer Aided Control Systems Design*, Taipei (TW), September 2004, pp. 284–289.

[26] E. J. Kelly, "An adaptive detection algorithm," *IEEE Transactions on Aerospace and Electronic Systems*, vol. 22, pp. 115–127, March 1986, issue n.2.

[27] A. De Maio, A. De Nicola, A. Farina, and S. Iommelli, "Adaptive detection of a signal with angle uncertainty," *IET Radar, Sonar & Navigation*, vol. 4, pp. 537–547, August 2010, issue n.4.

[28] S. Boyd and L. Vandenberghe, *Convex optimization*. Cambridge University, 2003.